# Computational Aerothermodynamic Environments for the Mars 2020 Entry Capsule

Adam J. Wise*
*NASA Langley Research Center, Hampton, VA, 23681*

Dinesh K. Prabhu† and David A. Saunders‡
*Analytical Mechanics Associates, Inc., Moffett Field, CA, 94035*

Christopher O. Johnston§ and Karl T. Edquist¶
*NASA Langley Research Center, Hampton, VA, 23681*

**The simulation tools and processes used to generate aerothermodynamic environment definitions for the Mars 2020 entry capsule are presented. The Mars 2020 capsule leverages the heritage Mars Science Laboratory design, but the entry will follow a different trajectory, landing at a different location and altitude on Mars. The general strategy for creating the Mars 2020 mission-specific environments follows from the Mars Science Laboratory experience. The primary difference is that now the effects of shock-layer radiation are modeled, with particular concern for the backshell.**

## I. Nomenclature

| | |
|---|---|
| $P$ | static pressure, Pa |
| $Q$ | heat load (time-integrated heat rate), J/cm$^2$ |
| $q$ | heat rate, W/cm$^2$ |
| $q_\infty$ | free stream dynamic pressure, Pa |
| $T$ | temperature, K |
| $x$, $y$, $z$ | Cartesian coordinates, m |

*Subscripts*

| | |
|---|---|
| $_{conv}$ | convective component |
| $_{rad}$ | radiative component |

## II. Introduction

NASA's Mars Science Laboratory (MSL) mission[a] successfully landed the Curiosity rover on the Martian surface on August 6, 2012. The success of MSL has led NASA to a sister mission, with updated science instruments on the new rover, the Mars 2020 mission,[b] with a launch window between July and August of 2020. To help reduce cost, risk, and schedule, Mars 2020 retains as much of the MSL design heritage as possible. Relevant to the present report, the Mars 2020 entry capsule thermal protection system (TPS) and outer mold lines match MSL.

However, Mars 2020 will have a different entry trajectory than MSL, delivering its rover to a different location on Mars, and so the MSL-heritage TPS design must be verified as sufficient for use on the Mars 2020 trajectory. In order to perform the thermal protection verification analyses, a data set of mission-specific aerothermodynamic environments are needed for the Mars 2020 entry capsule. These environments are primarily in the form of surface pressures and heat transfer rates as functions of trajectory point and angle of attack.

*Aerospace Engineer, Aerothermodynamics Branch, M/S 408A.
†Senior Scientist, Entry Systems and Technology Division, M/S 229-3, Associate Fellow.
‡Senior Research Scientist, Aerothermodynamics Branch, M/S 230-2, Senior Member.
§Aerospace Engineer, Aerothermodynamics Branch, M/S 408A, Member.
¶Aerospace Engineer, Atmospheric Flight and Entry Systems Branch, M/S 489, Senior Member.
[a]`https://mars.nasa.gov/msl/`
[b]`https://mars.nasa.gov/mars2020/`

This paper documents the computational tools and techniques, along with sample data, that produced the aerothermodynamic environments for the Mars 2020 TPS verification. The database construction process was largely the same as has been previously reported for MSL[1], with three differences incorporated reflecting advancements in the state of the art. The primary difference is the inclusion of shock-layer radiation modeling; the other differences are an incrementally updated flow solver and increased geometric resolution, afforded by advancements in supercomputing power.

## III. Procedure

The procedures for performing the numerical flow field simulations for the Mars 2020 entry capsule follow on from the best practices and lessons learned during the MSL mission[2]. The aerothermodynamic database was constructed entirely from numerical simulations, and as a risk reduction two independent sets of simulation toolsets were utilized, with selected duplication performed as verification. This section presents the simulation tools, the Mars 2020 entry capsule geometry, the mission-specific trajectory, and the simulation procedures.

### A. Simulation suite LAURA 5 and HARA

Thermal verification environments for Mars 2020 were produced in part using the Langley Aerothermodynamic Upwind Relaxation Algorithm version 5 (LAURA 5) [3] and the High-temperature Aerothermodynamic RAdiation code (HARA) [4]. LAURA 5 is a second-order accurate, finite-volume, viscous, thermochemical nonequilibrium flow solver for structured grids. The LAURA flow solver has a rich heritage of providing convective heating environments for Mars missions, including MSL, for which version 4 was available at the time. LAURA 5 was a Fortran 95 update to version 4, retaining the same numerics and gas-physics. LAURA 5 additionally has the updated $CO_2$ kinetics necessary for shock-layer radiation calculations in conjunction with the HARA code for both coupled and uncoupled radiation calculations.

HARA is a shock-layer radiation code, including atomic line and continuum models, and molecular band systems. It includes models for line-by-line, smeared-rotational band, and a new multiband opacity-binning option that has shown at least an order of magnitude speed-up compared to the line-by-line method. HARA uses the tangent-slab approach to calculate the radiative flux at a surface point or any collection of points. This approach is sufficient for the relatively thin shock layer around the heatshield, but not on the backshell where a single surface-normal line-of-sight does not accurately approximate shock-layer radiation contributions from wall-oblique directions. Ray-tracing is therefore applied to provide accurate radiative heating predictions in non-tangent-slab like regions of the flow.

### B. Simulation suite DPLR and NEQAIR

The Data Parallel Line Relaxation Code (DPLR) version 4.04 [5] and Nonequilibrium Radiative Transport and Spectra Program (NEQAIR) version 14 [6] were utilized to independently verify and validate the LAURA 5 and HARA results. DPLR is a finite-volume Navier-Stokes solver with third-order numerics for solving block structured grids in parallel in distributed memory computational environments. Like LAURA 5, DPLR includes models for finite-rate chemical kinetics, thermal and chemical nonequilibrium, ionized flow physics, high-temperature transport properties, and various surface catalysis and wall boundary conditions. DPLR is able to interface with the NEQAIR shock-layer radiation code.

NEQAIR utilizes the line-by-line method to compute the radiation transport within a flowfield to a point on a vehicle along a line-of-sight from that surface point. This can be done using the tangent-slab approximation or full-angular integration. DPLR and NEQAIR work side-by-side with LAURA 5 and HARA as NASA's premier hypersonic entry codes. They have been used most recently on NASA's InSight mission.

### C. Capsule geometry and domain grid

A graphic of a simplified, smooth outer mold line of the Mars 2020 capsule is shown in Fig. 1. Just like MSL, the capsule has a 4.5 meter diameter sphere-cone heatshield. The heatshield TPS material is made of Phenolic Impregnated Carbon Ablator (PICA) tiles with gaps filled to inhibit inter-tile gas flow. There is a step at the heatshield-backshell transition and a seal at the juncture. This step was not modeled in MSL calculations, but is included in Mars 2020 environments. The main biconic portion of the backshell is protected by Super Lightweight Ablator (SLA-561V) material. The final truncated cone, parachute closeout cone (PCC), and the backshell interface plate (BIP) at its base are covered by a low-density silicone syntactic foam called Acusil® II.

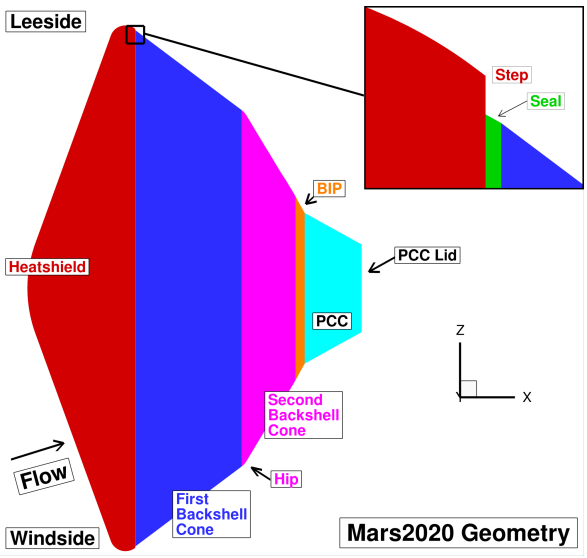


**Fig. 1 Mars 2020 Geometry with Labels.**

LAURA 5/HARA and DPLR/NEQAIR utilized two independently generated grid systems. Both systems are point-matched, multiblock structured grids that have been built to be load balanced at runtime. Additionally, LAURA 5 and DPLR were both used to tailor the outer grid boundary to the shock and cluster the off-wall normal cells to allow for appropriate boundary layer resolution for each flowfield condition. The LAURA 5 grid is 80 blocks, each having an $11 \times 11$ points per surface patch for the coarsened version (shown in Fig. 2a), and 129 points in the wall-normal direction. This is a similar surface density to what was used for most of the MSL simulations. The number of wall normal points has doubled to assure appropriate grid density for backshell shock-layer radiation calculations. It is also a best-practice to leave the the wall normal clustering at the shock intact after grid tailoring to allow sufficient shock-layer resolution for radiation calculations. Figure 2b displays the fine surface grid level used for DPLR/NEQAIR simulations. The DPLR grid has 100 grid points in the radial direction, versus 41 for LAURA 5. The LAURA 5 grid system has 211 surface points axially distributed, where the DPLR grid includes 407. Both grids share a wall-normal resolution of 129 points.

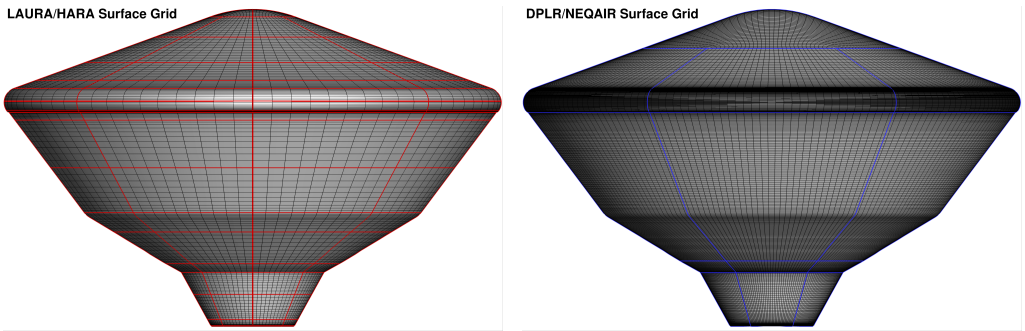


**(a) LAURA 5/HARA Surface Grid** **(b) DPLR/NEQAIR Surface Grid**

**Fig. 2 Surface Grids.**

## D. Trajectory

The design trajectory for Mars 2020 thermal environments is 15-TPS-01. This trajectory has the highest entry speed in the capsule's arrival space and long thermal response times due to the low altitude traversal of the atmosphere during entry. For these reasons, it was thought to be the most stressing trajectory for the estimation of thermal environments. There are eighteen points chosen along the 15-TPS-01 trajectory to encapsulate the heat pulse (Fig. 3a) for the CFD simulations. These points are tabulated in Fig. 3b, and the case numbers will be referred to in the results section of this paper. Capturing the heat pulse in the simulation space was important, because the height and breadth of the thermal environment at key body points on the vehicle were used to validate the design of the Mars 2020 thermal protection system.

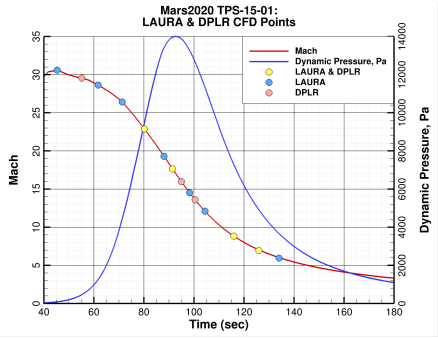


**(a) Mach number and dynamic pressure with selected trajectory points.**

| Case# | Time s | Vel. $m.s^{-1}$ | Dens. $kg.m^{-3}$ | Temp. K | AoA deg | Mach | LAURA/ DPLR |
|---|---|---|---|---|---|---|---|
| 1 | 45.315 | 5552.2 | 0.00000555 | 131 | 16.276 | 30.58 | LAURA |
| 2 | 55.16 | 5546.2 | 0.00002990 | 140 | 15.012 | 29.55 | DPLR |
| 3 | 61.685 | 5455.9 | 0.00008440 | 144 | 15.260 | 28.63 | LAURA |
| 5 | 71.325 | 5270.4 | 0.00032000 | 158 | 15.614 | 26.41 | LAURA |
| 7 | 4856.8 | 4856.8 | 0.00080100 | 179 | 15.6 | 22.88 | Both |
| 9 | 88.005 | 4227.1 | 0.00150000 | 190 | 15.886 | 19.3 | LAURA |
| 10 | 91.455 | 3895.4 | 0.00184000 | 193 | 15.9 | 17.64 | Both |
| 11 | 95 | 3551.1 | 0.00220000 | 196 | 16.070 | 15.97 | DPLR |
| 12 | 98.235 | 3245.7 | 0.00252000 | 198 | 16.409 | 14.52 | LAURA |
| 13 | 100.47 | 3045.5 | 0.00273000 | 199 | 16.615 | 13.59 | DPLR |
| 14 | 104.4 | 2722.2 | 0.00306000 | 201 | 16.811 | 12.1 | LAURA |
| 16 | 115.930 | 2000.0 | 0.00364000 | 203 | 17.2 | 8.83 | Both |
| 17 | 125.940 | 1591.7 | 0.00386100 | 204 | 17.6 | 6.927 | Both |
| 18 | 134 | 1366.7 | 0.00392540 | 204 | 17.679 | 5.945 | LAURA |

**(b) Tabulated trajectory points**

**Fig. 3 15-TPS-01 trajectory with CFD points.**

## E. Methodology

The flow solvers were set up to model the Mars atmosphere utilizing 8-species ($CO_2$, CO, $N_2$, $O_2$, NO, C, N, O); LAURA 5 utilized updated Johnston and Brandis[7] kinetics and DPLR used Mitcheltree[8] chemistry. Both codes were run in thermochemical nonequilibrium with supercatalytic surface recombination on the heatshield, step, seal and biconic sections of the surface (forces all 8 species to free stream concentrations at the wall), and the radiative-equilibrium wall temperature boundary condition. LAURA 5 calculations used a constant emissivity value of 0.89 (MSL heritage) and DPLR used 0.85. The BIP and PCC surfaces were modeled as noncatalytic. Unless otherwise noted, forebody solutions are modeled as fully turbulent (algebraic Baldwin-Lomax) and backshell environments are modeled as laminar. Forebody radiative heating used the tangent-slab approach and all backshell radiation calculations were computed using ray-tracing integration. NEQAIR used the line-by-line approach and HARA results were achieved using the new multiband opacity-binning approach. Radiative flux was calculated in the $CO_2$ and CO infrared band systems. (The CO 4th-Positive band was checked on the heatshield and backshell and shown to be negligible.)

## F. Convergence Criteria

Aerothermodynamic simulation best practices were used to reach appropriately converged flowfield and surface results. These best practices include, but are not limited to:

- tailoring grid to the shock
- clustering the near wall grid and setting the first off-wall grid spacing so that the Reynold's number within the cell is of order(1)
- for backshell shock-layer radiation calculations the outer boundary needs to be about 5-7 vehicle diameters downstream to capture a realistic amount of $CO_2$ that is still radiating in the wake [9].
- (LAURA 5) setting the radiative equilibrium wall relaxation factor to near default value
- (LAURA 5) finish convergence cycle of the attached flow regions using line-implicit
- (steady flowfield using local time-stepping) run the simulations out until the surface heating (in attached regions)

does not change (within a minimum threshold over a specified iteration range), it appears to be sufficiently converged numerically and surface heating contours are smooth
- (unsteady flowfield using global time-stepping) the same as the steady flowfield convergence, but using running means of surface results instead of instantaneous solutions

## IV. Results

A subset of results from CFD simulations for the Mars 2020 OML will be shown and discussed. All results are nominal (unmargined). There will not be any details about uncertainties, margin policies, or thermal sizing location selection as those topics are discussed elsewhere. Also, the aerothermal environments for MSL have been very well characterized and discussed by Edquist [1]. This paper will focus on computation of aerothermal environments for the smooth-OML and, mainly, on what is different from MSL; the flow solver, trajectory, geometry, and inclusion of radiation. Additionally, discussing computations on vehicle protuberances, specifically the radomes on the PCC, is beyond the present scope of this manuscript. Finally, DPLR was used to complete various parametric studies concerning surface catalycity, chemical kinetics and turbulence margining on the backshell. These studies added value to the understanding of the environments of the capsule and how to use the baseline data, but are also beyond the scope of this paper.

As was mentioned previously, radiative heating was not specifically modeled for the MSL design. So, the inclusion of radiation here is perhaps the pinnacle of Mars 2020 aerothermal considerations. When the task of estimating shock-layer radiation for Mars 2020 began, the question was whether the reduction in entry speed would offset the addition of radiation in the design validation aerothermal environments.

### A. Solvers

It is important to establish that LAURA 5 is providing similar results to the heritage code for a given set of trajectory conditions. Figure 4a shows the maximum surface heat rate among all turbulent trajectory conditions at each pitch plane centerline location on the heatshield. This figure shows that LAURA 5 produces maximum heat rates within 5% of the LAURA 4 result at most locations along the centerline. The exception to this is just to the leeside of the nose, between about 0.25 and 1.0 meter on the z-axis. One LAURA 5 solution displayed a strange heating character there, but it does not affect the location on the heatshield used for TPS sizing on the flank of the leeside cone (marked in the figure with the vertical line segment). At this location, the simulations from the codes are nearly identical. The integration of all heat rate data through the 15-TPS-01 trajectory, Fig. 4b, shows similar agreement. The problem on the leeside of the nose is less obvious, because it is only one part of the integrated whole.

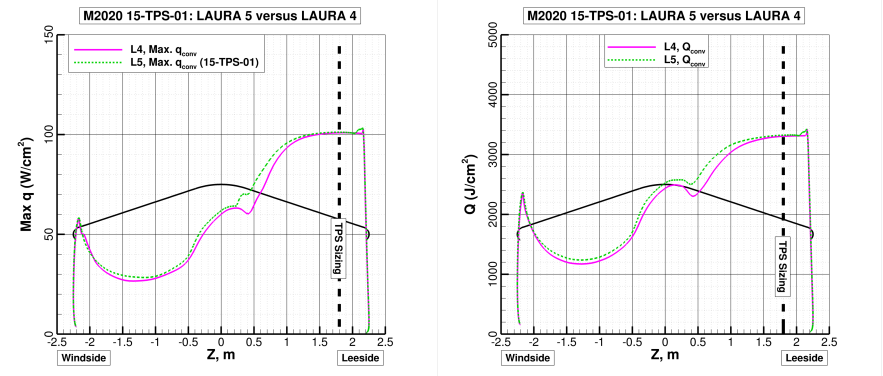


**(a) Maximum Heat Rate** **(b) Heat Load**

**Fig. 4 15-TPS-01 Trajectory Comparison: Heatshield (Turbulent).**

A similar set of plots is shown for the backshell, laminar trajectory conditions (Fig. 5). Notice in the legend that the LAURA 5 (green curve) and second set of LAURA 4 results (red curve) were solved on the same updated grid system utilizing the latest Mars 2020 CAD. Additionally, the grids were adapted using LAURA 5 and were unchanged for the LAURA 4 runs. The first set of LAURA 4 results (magenta curve) were solved on the older MSL grid system based on

OML-13F CAD. The comparison between LAURA 5 and LAURA 4 is valid on the shoulder transition, first backshell cone, hip and second backshell cone, but not on the BIP or PCC. For the LAURA 5 simulations, the regions on the plots bracketed by the vertical, green dash-dot line segments have a noncatalytic wall boundary condition. The LAURA 4 results are based on the supercatalytic model in this region. Additionally, the LAURA 5 surface results are averaged over several thousand global time-stepping iterations, while the LAURA 4 data are instantaneous results from simulations utilizing inconsistent time-steps. This difference can be seen in the higher frequency of local peaks-valleys in the LAURA 4 data. This divergence in run practices between these flow solvers persists for all other backshell LAURA 5 comparisons in this paper. Within the regions of applicability, the three solutions are very similar. The LAURA 5 result is just slightly more conservative near the seal and along the first backshell cone than the LAURA 4 result on the updated grid system (red curve). Also, in the solutions that utilize the latest Mars 2020 CAD in the surface grid (green and red curves), the drop in heating and then subsequent peak, is due to the step and associated recirculation region just downstream of the backward face. The MSL grid that was based on OML-13F does not model the step, though it was physically present on MSL. Instead, the grid models a tangent intersection between the shoulder and first backshell cone. The agreement on the windward and leeward of the second backshell cone, where separation and unsteady flow occur, give evidence that the two codes share a numerical heritage.

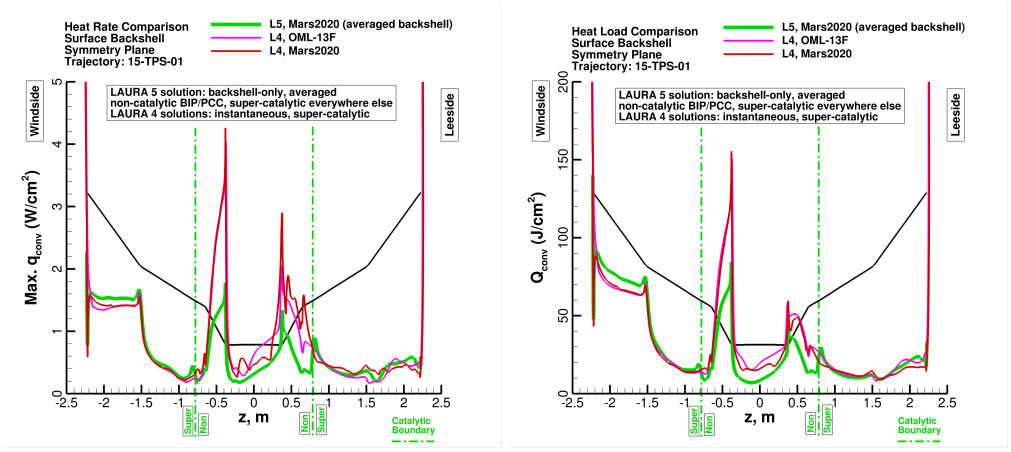


**(a) Maximum Heat Rate** **(b) Heat Load**

**Fig. 5 15-TPS-01 Trajectory Comparison: Backshell (Laminar).**

Figure 6 shows that the DPLR and LAURA 5 flow solvers to agree well for laminar simulations of blunt heat shields. The surface pressures on the pitch plane centerline are within 1%. Likewise, the surface heating matches very well, being less than a 10-percent difference everywhere on the heatshield. The character of the heating trends are also very similar, with the exception of some difference on the flanks and right at the nose. These types of differences have been seen before, and are not unexpected given two independent grids (surface, volume, shock alignment differences) and flow solvers. The scale of these plots does not allow much detail to be seen on the backshell, but that region will be looked at in more detail.

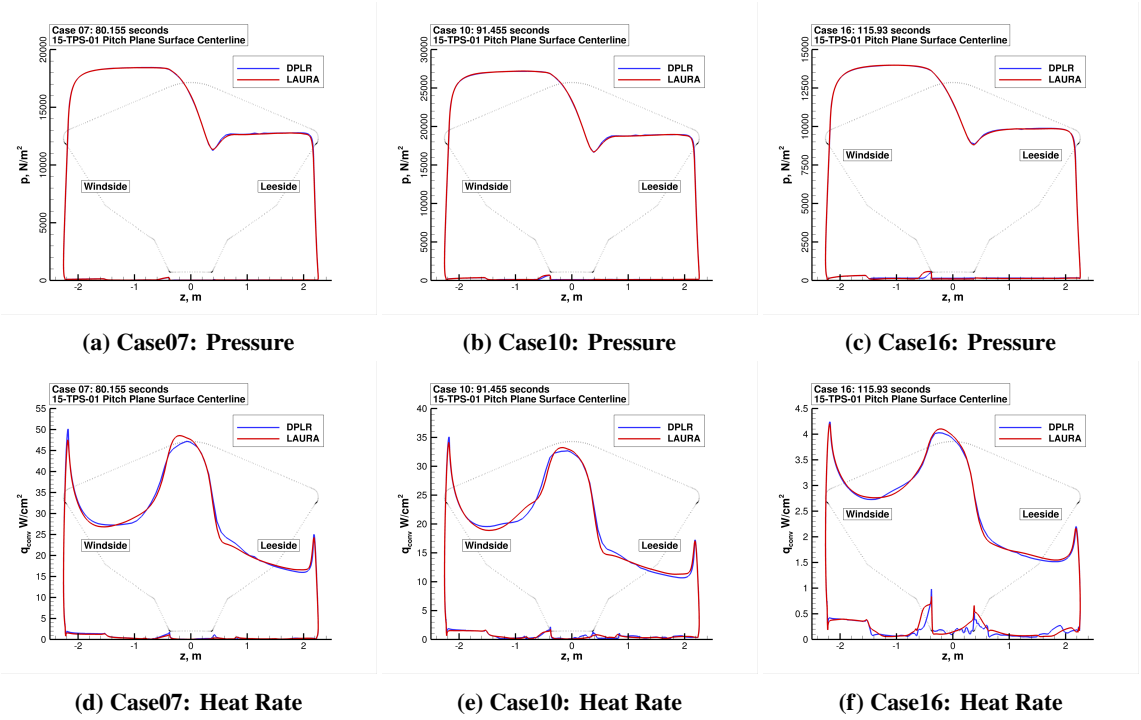


**(a) Case07: Pressure** **(b) Case10: Pressure** **(c) Case16: Pressure**

**(d) Case07: Heat Rate** **(e) Case10: Heat Rate** **(f) Case16: Heat Rate**

**Fig. 6 Heatshield Surface Centerline:** LAURA 5 **versus** DPLR**.**

## B. Trajectory

The trajectory used for TPS design on MSL was 09-TPS-01. This was the maximum heat load trajectory for the 2011 launch opportunity. The design trajectory for Mars 2020, 15-TPS-01, has a slower entry speed and traverses through lower, denser atmosphere for much of the heat pulse than 09-TPS-01. Because stagnation point heating scales as free stream velocity cubed, the heat load on the forebody is estimated to be lower than MSL design environments. The heating on the backshell, however; typically scales more closely with dynamic pressure, and 15-TPS-01 does have an overall higher dynamic pressure than 09-TPS-01, see Fig. 7.

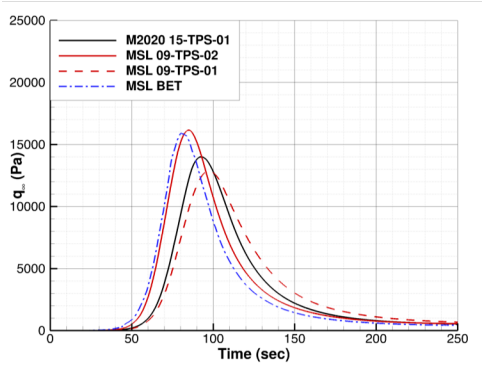


**Fig. 7 MSL and Mars 2020 Trajectory Comparison.**

Figure 8 shows that overall maximum convective heat rate on the Mars 2020 (15-TPS-01) heatshield is lower than for the MSL trajectory. This is true everywhere, except for the leeside of the nose, but again, that is not where the TPS is being maximally stressed. This is the result that was anticipated based on the what was known about 15-TPS-01 compared to 09-TPS-01. Figure 9 shows that the heating on the backshell (outside of the noncatalytic region) is higher on the first backshell cone on the windside for 15-TPS-01, displaying that backshell heating does predictably scale with dynamic pressure for this capsule.

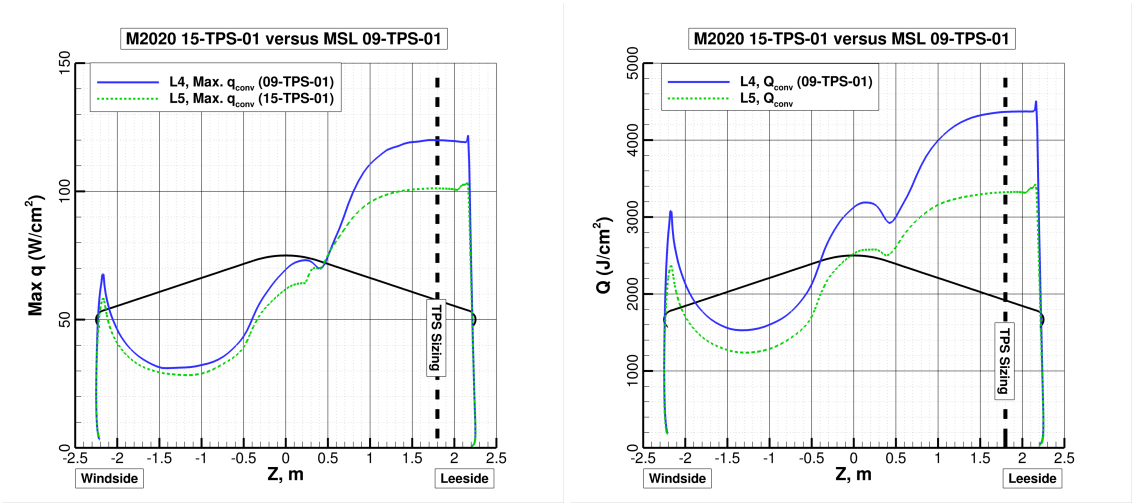


**(a) Maximum Heat Rate** **(b) Heat Load**

**Fig. 8 Heatshield Trajectory Comparison: 15-TPS-01 versus 09-TPS-01.**

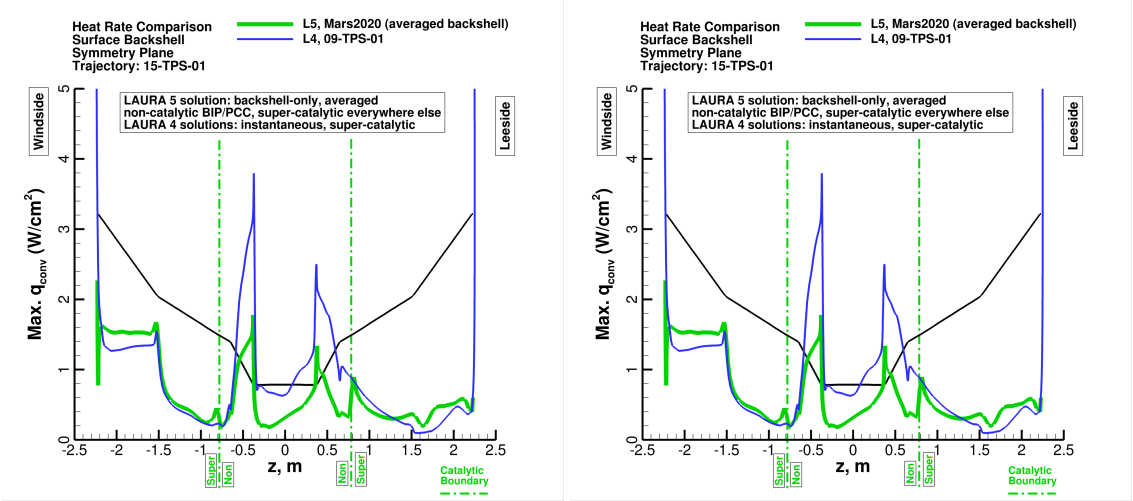


**(a) Maximum Heat Rate** **(b) Heat Load**

**Fig. 9 Backshell Trajectory Comparison: 15-TPS-01 versus 09-TPS-01.**

### C. Geometry

The block-structured MSL grids were based on CAD from OML-13F. The Mars 2020 computational grids were built based on a slightly updated Mars 2020 CAD file. The updated CAD includes a very late MSL design change to the Parachute Closeout Cone (PCC) lid where the lid TPS material thickness ramps down toward the middle of the lid, creating a slight concavity. Angle changes between the BIP and PCC are also included as shown in Fig. 10. It was desirable to update the surface grid topology and volume grid to match these changes and to also include the step that exists between the termination of the heatshield and first backshell cone.

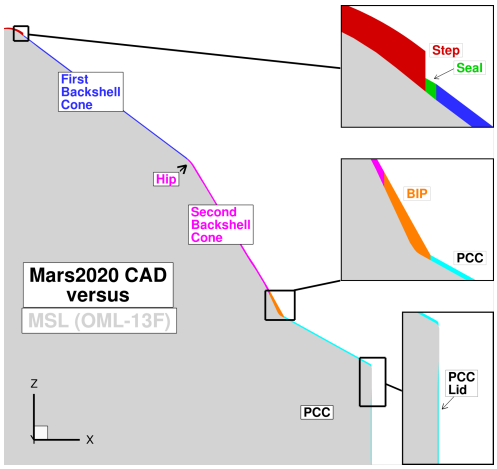


**Fig. 10 Mars 2020 CAD versus MSL (OML-13F) CAD.**

The largest meaningful difference between LAURA 5 and DPLR is observed just downstream of the backward facing step; Fig. 11. There is a small region of recirculating flow here (shown in Fig. 12), and a twenty-percent difference in heating between the two codes is seen where the flow reattaches. Case 10 is displayed, but a similar difference in heating trend exists in Case 07 and, to a lesser extent, Case 16. Even considering the separated flow at the base of the step, this is an area where the codes would be expected to agree well. The adverse pressure gradient also suggests a heating peak. For this reason, this discrepancy is being actively investigated, but conclusions have not been reached. This peak is the location used for thermal environment verification of the backshell seal (the junction between the heatshield and backshell TPS at the base of the step). The seal itself is upstream of the flow reattachment point, where the heating is lower. Additionally, the supercatalytic model is used here, and is conservative. Simulations were performed with DPLR utilizing the more realistic fullycatalytic model, and heating was shown to be less than the LAURA 5 peak for the Case 10 trajectory condition.

Moving on from the step, other differences do exist between the flow solvers on the backshell. The flow separates on the second cone on the windside and LAURA 5 separates first. There are differences in the grids and in the numerics between the codes, and those two factors play a big part in the solutions here. The DPLR code does show consistently higher heating on the windward PCC corner. There is a recirculating bubble in the flow field that sits above the PCC lid. This directly affects where the peaks occur on the leeward PCC cone.

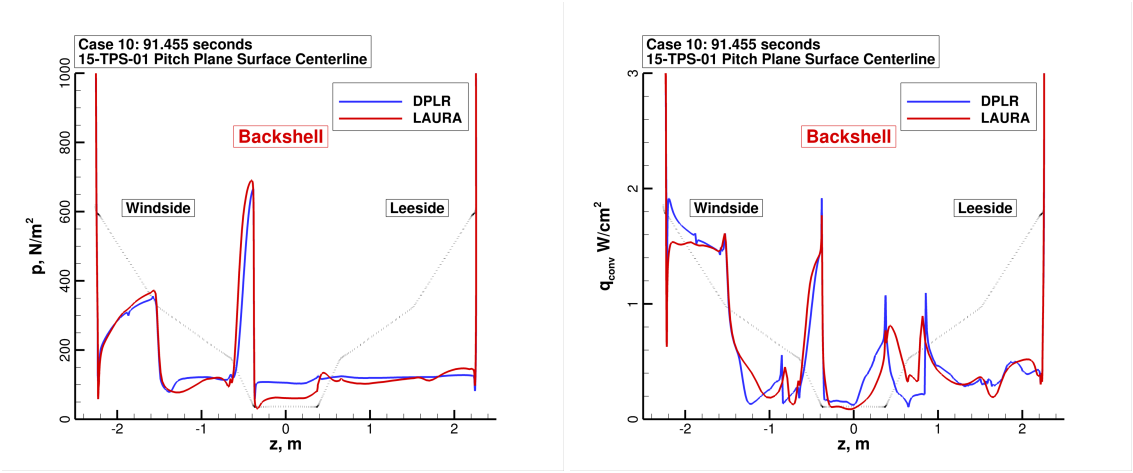


**(a) Pressure** **(b) Heat Rate**

**Fig. 11 Backshell Surface Centerline: LAURA 5 versus DPLR.**

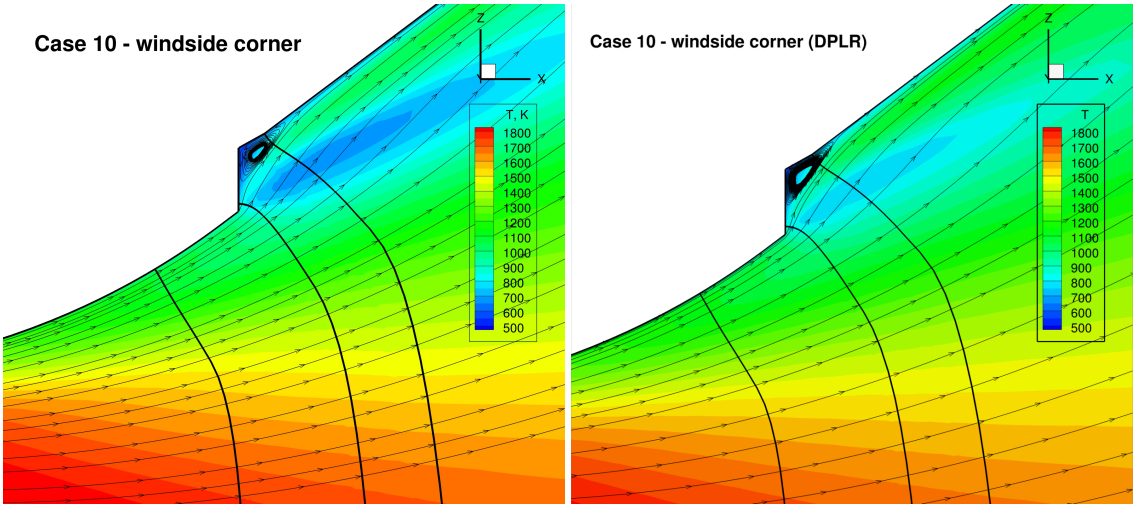


**(a)** LAURA 5 **(b)** DPLR

**Fig. 12 Pitch Plane Windside Step: Streamlines with Temperature Contours.**

### D. Radiation

Radiative heating estimates were not included in the design of the MSL TPS. The accuracy of radiative heating predictions on the backshell of capsule geometries has increased due to significant advances in modeling capabilities. The largest contributor to radiative heating is believed to be $CO_2$, specifically in the midwave infrared bands [9]. The radiative intensity of $CO_2$ at the frequencies and temperatures associated with Mars 2020 entry conditions has been modeled by current state-of-the-art shock layer radiation codes and validated by ground test data [10]. This capability includes implementation of ray-tracing computations of the radiative heating, which removes the tangent-slab approximation. Full angular integration applies contributions from radiating species from within a specified solid angle inside the flowfield to the specified surface point. Previously, only a single line of sight was used. This ability can be particularly important on the backshell of a entry capsule, where single-line-of-sight tangent slab calculations cannot account for contributions from a highly nonuniform flowfield [11]. Based on these computational predictions and the ground-test validation of $CO_2$ radiation [12], it was deemed important that radiation estimates be included in the Mars 2020 aerothermal verification environments predictions, both for the forebody and backshell.

The ray-tracing results on the backshell from HARA and NEQAIR, Fig. 13, compare well. Only the windside BOP location shows HARA to be consistently and substantially higher than NEQAIR. The speed-up gained from the new multiband optical-binning model in HARA afforded the ability to run ray-tracing at every point on the backshell. This offered a flexible way to look for combined convective-plus-radiative local heating peaks in TPS regions of interest. The benefit of this approach can be seen for the other three backshell locations that are compared. Even though the results show good agreement, the true local peaks (for HARA) occur at slightly different locations than what were previously defined for thermal analysis based on earlier CFD simulations.

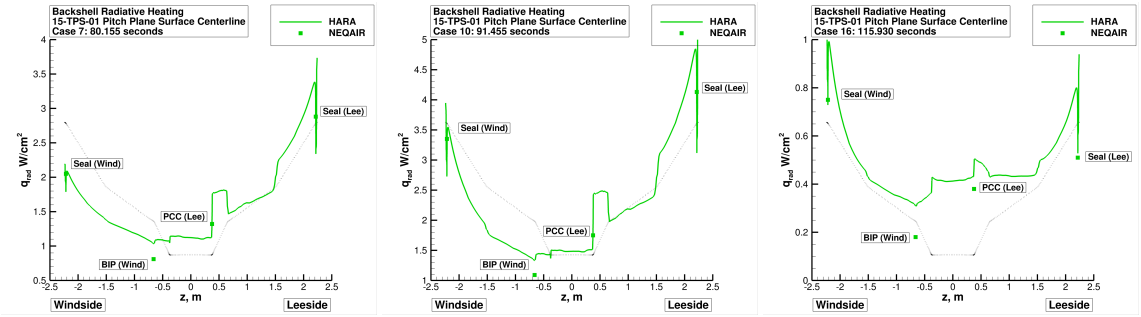


**(a) Case07** **(b) Case10** **(c) Case16**

**Fig. 13 Backshell Centerline Radiative Heating Comparison: LAURA 5 versus DPLR.**

Finally, adding the tangent-slab result to the heatshield convective heating estimates (Fig. 14), shows that the nominal Mars 2020 environments are less than the unmargined MSL design environments. For this portion of the TPS, the reduced entry speed of the Mars 2020 trajectory is predicted to offset the inclusion of shock-layer radiation estimates.

This is not the case, however; for the backshell. The heat load plot in Fig. 14 shows that radiative heating dominates the heat load levels for most of the backshell. This plot should only be used for qualitative purposes for two reasons: (1) The radiative heat load was integrated using a simple trapezoidal rule calculation, not curve fitting using the underlying trajectory conditions and timings. (2) This plot does not take margins into consideration. Uncertainties for laminar backshell convective heating data are much higher than for backshell shock-layer radiation utilizing full-angular integration. At least for the nominal heating data, it would appear that the reduction in Mars 2020 entry velocity does not offset the addition of radiative heating estimates.

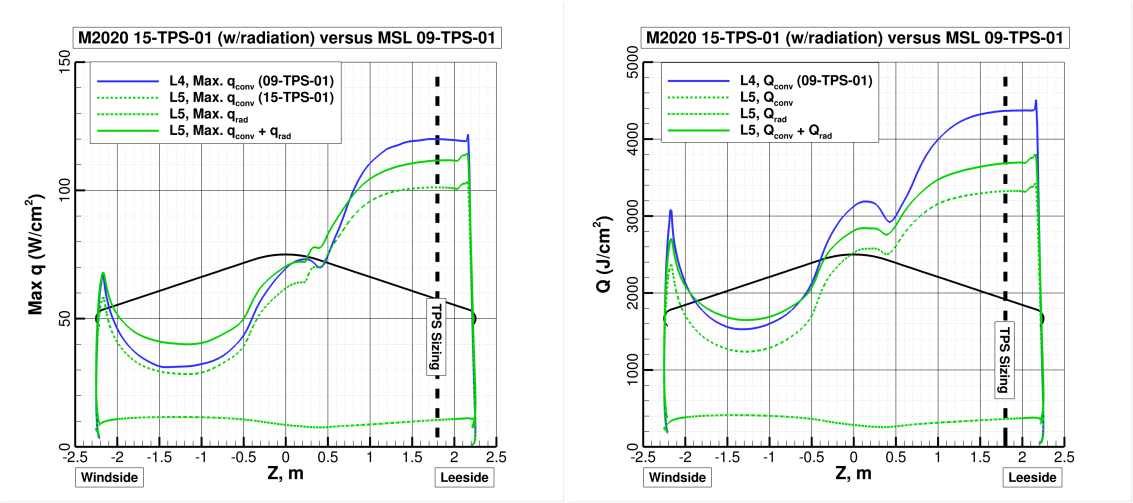


**(a) Maximum Heat Rate** **(b) Heat Load**

**Fig. 14 Heatshield Trajectory Comparison: 15-TPS-01 (with Radiation) versus 09-TPS-01.**

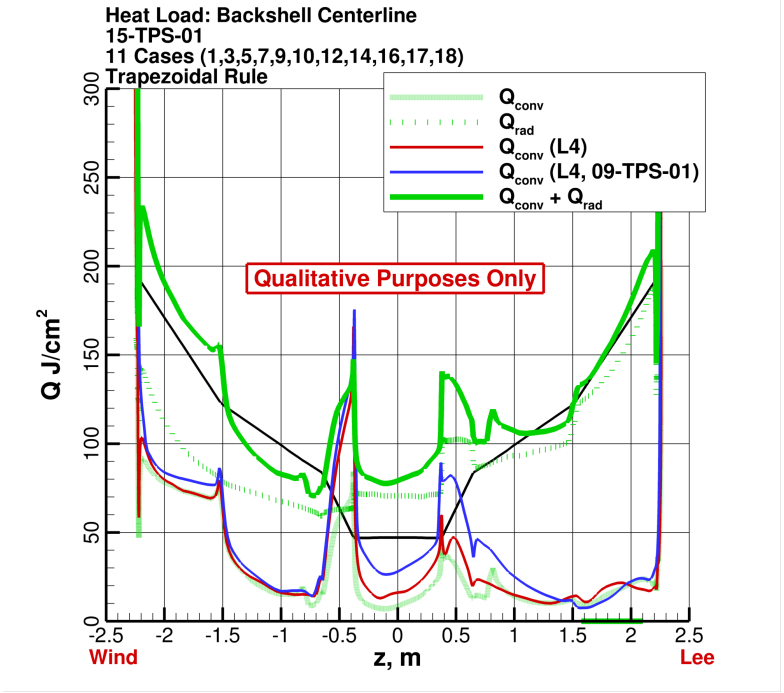


**Fig. 15 Backshell Trajectory Comparison: 15-TPS-01 (with radiation) versus 09-TPS-01.**

## V. Concluding Remarks

The Mars 2020 entry capsule inherits the Mars Science Laboratory (MSL) design, but is targeting a different landing site on Mars, with a consequent different entry trajectory than MSL. As part of the verification of the MSL-heritage thermal protection system on Mars 2020, a new database of entry aerothermodynamic environments has been generated corresponding to this mission-specific trajectory. The environments were generated by numerical simulations, and two sets of simulation tools were used, with overlap as a verification check. The simulation tools and the procedures for their application were described herein, generally following the best practices learned during the MSL experience. Of primary difference in simulation approach between MSL and Mars 2020 is the inclusion now of flow field radiation modeling. Additional, incremental differences between MSL and Mars 2020 approaches involve the use of the latest versions of the simulation tools and increased fidelity in geometry modeling, made practical by advances in computing power since the MSL development program.

## References


[1] Edquist, Karl T., et al., "Mars Science Laboratory Heat Shield Aerothermodynamics: Design and Reconstruction," J. of Spacecraft and Rockets 51(4), 1106-1124 (2014).

[2] Edquist, K. T., Dyakonov, A. A., Wright, M. J., and Tang, C.-Y., "Mars Science Laboratory Entry Capsule Aerothermodynamics Environments: Revision B," JPL Document D-34661-B, 8 November 2010.

[3] Mazaheri, A., Gnoffo, P., Johnston, C., and Kleb, B., "LAURA Users Manual," NASA TM 2010-216836, 2010.

[4] Johnston, C. O., "Nonequilibrium Shock-Layer Radiative Heating for Earth and Titan Entry," Ph.D. Dissertation, Virginia Polytechnic and State Univ., Blacksburg, VA, 24061.

[5] Wright, M., White, T., and Mangini, N., "Data-Parallel Line Relaxation (DPLR) Code User Manual Acadia-Version 4.01.1," NASA/TM-2009-215388, NASA Ames Research Center, October 2009.

[6] Cruden, B., Brandis, A., "Updates to the NEQAIR Radiation Solver" ARC-E-DAA-TN19271, NASA Ames Research Center, November 2014.

[7] Johnston, C. O., Sahai, A., Panesi, M., "Extension of Multiband Opacity-Binning to Molecular Non-Boltzmann Shock Layer Radiation," J. of Thermophysics and Heat Transfer, *accepted for publication* (2018).

[8] Mitcheltree, R., and Gnoffo, P., "Wake Flow About a MESUR Mars Entry Vehicle," AIAA Paper 94-1958, June 1994.

[9] Brandis, A. M., Saunders, D. A., et al., "Radiative Heating on the After-Body of Martian Entry Vehicles," 45th AIAA Thermophysics Conference, Dallas, Texas, 2015, AIAA 2015-3111.

[10] Jaffe, Richard, "Vibrational and Rotational Excitation and Dissociation of CO2 Reexamined," 49th AIAA Aerospace Sciences Meeting, Orlando, FL, 2011, AIAA-2011-447.

[11] Mazaheri, Alireza, et al., "Three-Dimensional Radiation Ray-Tracing for Shock-Layer Radiative Heating Simulations," J. of Spacecraft and Rockets 50(3), 485-493 (2013).

[12] Cruden, B., Prabhu, D., and Brandis, A., "Measurement and Characterization of Mid-wave Infrared Radiation CO2 Shocks," 11th AIAA/ASME Joint Thermophysics and Heat Transfer Conference, Atlanta, Georgia, 2014, AIAA 2014-2962.